Design of the Wind Turbine Airfoil Family RISØ–A–XX

Kristian S. Dahl, Peter Fuglsang

Abstract   A method for design of wind turbine airfoils is presented. The design method is based on direct numerical optimization of a B-spline representation of the airfoil shape. For flexibility, the optimization algorithm relies on separate, stand alone tools for the analysis of aerodynamic and structural properties. The panel method based XFOIL is used during the optimization whereas the Navier-Stokes solver EllipSys2D is used in the evaluation of the results.

The method is demonstrated by the design of an airfoil family composed of 7 airfoils ranging in thickness from 12% to 30%. The design is based on Reynolds and Mach numbers representative of a 600 kW wind turbine. The airfoils are designed to have maximum lift-drag ratio until just below stall, a design lift coefficient of about 1.55 at an angle of attack of 10° and a maximum lift coefficient of 1.65. The airfoils are made insensitive to leading edge roughness by securing that transition from laminar to turbulent flow on the suction side occurs close to the leading edge for post stall angles of attack.

The design method and the airfoil family provides a sound basis for further enhancing the characteristics of airfoils for wind turbines and to tailor airfoils for specific rotor sizes and power regulation principles.

Contents

1   Introduction

Design of tailored airfoils for wind turbine rotor blades is important for the continuing development of wind turbines. Optimization studies show that airfoils with suitable characteristics are important to further reduce the cost of the produced energy, Fuglsang and Madsen [13]. The airfoils that are currently used range from rather old NACA airfoil series originally developed for airplanes, Abbot and Doenhoff [1] to dedicated wind turbine airfoils. Wind turbine airfoils should differ from traditional aviation airfoils in choice of design point, off-design capabilities and structural properties.

The development of wind turbine airfoils has been ongoing since the mid 1980's and a large effort was done by Tangler and Somers [29], who developed several airfoil families. Other airfoil designs for wind turbines can be found in Björk [4], Timmer and van Rooy [30], Hill and Garrad [17] and Chaviaropoulos et al. [6]. Most of these airfoil designs were developed by use of inverse design methods.

Numerous methods for airfoil design are available and a survey of such methods and available references can be found in Henne [15] and Dulikravich [10]. In traditional inverse design, the airfoil surface flow is prescribed at specified operational conditions and a shape is found that will generate these surface conditions. Full-inverse methods determine the overall airfoil geometry from the overall surface pressure distribution whereas mixed-inverse methods determine parts of the airfoil contour while holding the rest unchanged.

A full-inverse approach for incompressible flows is the complex mapping method originally formulated by Mangler [22] and Lighthill [20]. A method that includes a boundary layer formulation is later developed by Liebeck [19]. On basis of these methods, Eppler and Somers developed their computer code [11], which has been used for development of numerous wind turbine airfoils, e.g., [29]. A popular mixed-inverse method is the XFOIL code by Drela [9] that uses a global Newton method. XFOIL was used for design of wind turbine airfoils by Björk [4] among others.

Traditional inverse design methods in general have limited capabilities for multiple design points, since there is only a single target pressure distribution at a single design point. However, a method for multi-point design using an inverse method was developed by Selig and Maughmer [27]. They allow different segments of the airfoil shape to be determined by different flow constraints. Inverse design methods can not treat multidisciplinary design problems and allow only limited off-design considerations. These matters are most often taken care of manually by the designer in a cut-and-try process.

Direct design methods based on numerical optimization provide basically a rational multidisciplinary design procedure where several design parameters can be improved and multiple constraints can be imposed. A general flow solver and eventually a structural code are coupled with a numerical optimization algorithm. The optimization algorithm generates an optimum airfoil shape that has desirable characteristics, as specified by the designer, while satisfying aerodynamic and structural constraints.

Most direct design methods use gradient-based algorithms. Hicks et al. [16] used a simple feasible direction algorithm with a panel method in their design of transonic airfoils. When a more complex flow solver is used, such as in Eyi and Lee, [12], the computational costs increase because of the sensitivity analysis, which requires a large number of analysis runs. In the case of Navier-Stokes or Euler solvers, computational costs can be reduced by the use of adjoint operator/control theory, Jameson [18]. Another category of methods are evolutionary algorithms such as in Obayashi and Takanashi [25] and stochastic approaches, Aly et al. [2].

They are less sensitive to local minima but have very high computational costs.

Airfoil design is a multidisciplinary field, involving aerodynamics, structural dynamics, stability and control, manufacturing and maintenance considerations. Despite available design methods, airfoil design remains to a great extent a cut-and-try procedure where advanced design methods assist the designer. The purpose of the present work was to further automate the airfoil design process by developing an interdisciplinary optimization method for airfoil design, which used a numerical optimization algorithm. The method relied on a state of the art tool for analysis of the flow field and included simple structural calculations. Attention was paid to the ability to design airfoils from scratch and a strategy for tailoring of wind turbine airfoils was developed. The design method was demonstrated by the design of an airfoil family for pitch- or stall-regulated wind turbines with a rated power around 600 kW.

2 Wind turbine airfoil characteristics

The characteristics of an ideal wind turbine airfoil depend in principle on the specific rotor the airfoil is intended for. But, in general, some properties can be labeled as desirable for most wind turbine airfoils.

For maximum power production, the lift-drag ratio should be high for airfoils used on the outer part of the blades. In case of pitch regulation and active stall regulation, the lift-drag ratio should be high at and near the operational point. For stall regulation, the lift-drag ratio should be high in the entire operational range, i.e., angle of attack below the maximum lift coefficient. On the inboard part of the blades, the lift-drag ratio is of less importance, but the maximum lift should be high to reduce the blade area.

The operational point should be close to maximum lift. This ensures high lift-drag below stall for stall regulation and in case of wind gusts for pitch regulation an autonomous stall control is build in to reduce power peaks.

Good off-design characteristics are important because of the wide variation in the angle of attack during normal operation (this is in contrast to aviation operating conditions). For stall regulation, the flow at maximum lift should separate from the trailing edge to have a smooth lift curve in stall which reduces the risk of stall induced vibrations in contrast to massive leading edge separation. The transition from the linear part of the lift curve to the post stall area should be well-defined and smooth. Furthermore, the airfoil should be insensitive to double stall, Bak [3].

In natural conditions, bugs and dirt often soil wind turbine blades at the leading edge. Roughness at the leading edge will cause early transition from laminar to turbulent flow and an eventual jump in the boundary layer momentum thickness. This reduces maximum lift, lower the lift curve slope and increase the skin friction resulting in loss of power production. Especially for stall regulation, the maximum lift coefficient should be insensitive to leading edge roughness.

On the inboard blade section, the airfoils should have high cross section stiffness, to limit blade weight and tip deflection. This is most easily obtained by increasing the airfoil maximum thickness at the expense of aerodynamic performance, e.g., reduced lift-drag ratio.

The desirable airfoil characteristics constitute both aerodynamic and structural properties and multiple conflicting characteristics are involved. High lift-drag is in contrast to high airfoil thickness. High maximum lift is in contrast to insensitivity to leading edge roughness. High lift-drag ratio at the design point is difficult to obtain together with extensive off-design requirements. But, this is exactly where numerical optimization is useful, because it can search the design space in a systematic manner and find the best compromise between these conflicting requirements. The designer of course still has to make qualified decisions on the relative weighting of the different desirable properties.

3 Design method

The design method is based on numerical optimization. The general formulation of an optimization problem is, e.g., [31]:

$$
\begin{aligned}
\text{Minimize:} \quad & F(\boldsymbol{x}) \\
\text{Subject to:} \quad & G_j(\boldsymbol{x}) \leq 0, \qquad j = 0,\, m
\end{aligned}
$$

where $m+1$ is the number of constraints. The objective function, $F(\boldsymbol{x})$, is minimized by changing the design variables that compose the design vector, $\boldsymbol{x}$. Here, the design variables are the coordinate points that describe the airfoil shape. The inequality constraints, $G_j(\boldsymbol{x})$, are side values for the design variables and bounds on response parameters. Equality constraints can be replaced with two inequality constraints with opposing signs.

3.1 Design algorithm

The combination of numerical optimization and different tools for flow and structural calculations are shown in Figure 1.
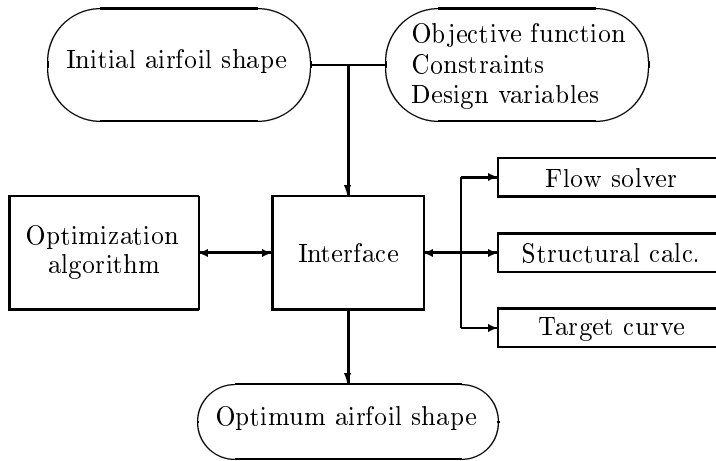
Figure 1. Flow chart of the design method.

An airfoil shape (in principle, any airfoil-like shape) is input together with a definition of the objective function, the design variables and the constraints. The optimization process is iterative and the iteration loop involves several calculations of flow and structural properties. Different tools carry out these tasks. An interface handles the necessary book-keeping of design variables and constraints and the calculation of sensitivity information. The interface converts the actual design vector into an airfoil shape. The flow and structural calculations are used to estimate the value of the objective function and the constraints. Multiple angles of attack can be calculated to allow off-design optimizations and the combination of flow and structural responses allows interdisciplinary optimization. When available, other calculation tools, such as calculation of aerodynamic self noise can easily be incorporated. Traditional inverse airfoil design is made possible by comparing the actual flow response with prescribed target values.

3.2 Geometry description

A smooth airfoil shape is important for the optimization results. In principle, any physically realistic shape should be possible to allow design from scratch. The shape description should have as much geometric flexibility as possible with as few design variables as possible to secure an effective and representative search of the design space with acceptable computational costs. It is important that the geometric description does not limit the design space too much a priori. Different approaches can be used. Hicks et al., 1974 [16] describe the airfoil thickness by a polynomial where the coefficients are design variables. Others such as [5] represent the airfoil surface by polynomials. An initial airfoil shape can be modified by adding smooth perturbations as in [14] where a linear combination of a set of base functions is used with weighting coefficients as design variables. However, these methods need a large number of design variables to have sufficiently geometric degrees of freedom and this increases computational costs and might cause scatter in the airfoil geometry.

In the present case, the airfoil shape is represented by a single B-spline curve defined by a set of control points [7]:

$$\boldsymbol{p}(u) = \sum_{i=0}^{n} \boldsymbol{P}_i N_{i,k}(u)$$

where $0 < u < n - k + 2$, k is the order of continuity, $P_i(\eta_i, \xi_i)$ are the coordinate points, $n + 1$ is the number of coordinate points, $N_{i,k}(u)$ are influence functions.

The B-spline curve was defined clockwise from the airfoil trailing edge and the airfoil shape was transformed into a standard $x - y$ coordinate system with the chord along the x-axis. The B-spline curve is continuous of the k'th order and no special considerations are necessary for the airfoil nose region. B-splines, furthermore, have the advantage that k determines how large a part of the entire curve that is altered when a single control point is moved. High values of k result in a smooth curve, whereas small values of k create a more lively curve. Figure 2 shows an example with $n + 1 = 12$, $k = 5$, which were common values for the present study. Most of the control points were only allowed to move in the y direction, which limits the number of design variables to be close to $n + 1$.
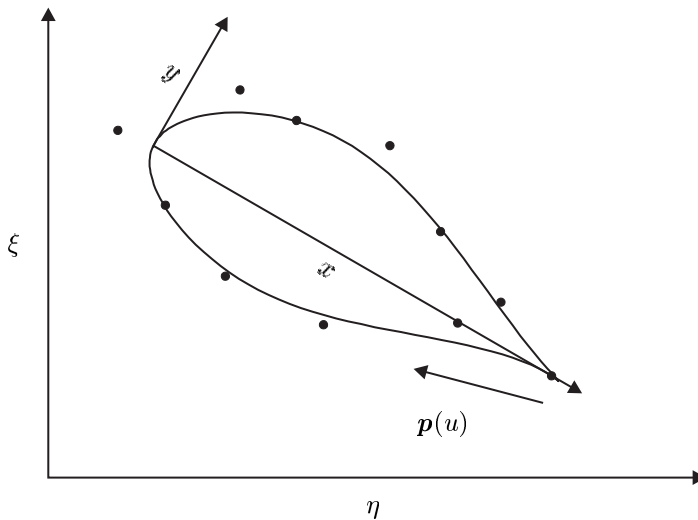

Figure 2. B-spline representing the airfoil shape, $n + 1 = 12$, $k = 5$. the dots are the control points/design variables.

3.3 Optimization algorithm

The choice of optimization algorithm is basically a choice between gradient based methods and global methods such as evolutionary type algorithms. Evolutionary algorithms are less sensitive to local minima. However they are time consuming and constraints have to be included as a penalty term on the objective function. Gradient based methods on the other hand allow multiple constraints but lack global optimality.

We chose a traditional simplex optimization algorithm based on sequential linear programming with move limits in a standard bound formulation [26]. Simplex methods are search method that are simple, robust and reasonably fast. They require the gradients of the objective function and of the constraints which are provided by a sensitivity analysis.

3.4 Sensitivity analysis

Adjoint operator/control theory methods have recently been applied to fluid flow equations [18]. This approach requires the additional solving of adjoint equations. Compared to traditional numerical finite differences, these methods are time saving when the number of design variables is large. However, the adjoint equations have to be derived for each of the governing flow equation.

We based the sensitivity analysis on numerical finite differences. This was more time consuming, but ensured flexibility in the choice of flow solver and structural calculations.

3.5 Flow analysis

In principle, there are no restrictions on the choice of flow solver. Since the optimization process requires many evaluations of the objective function and the constraints before an optimum design is obtained, computational costs are high when a Navier-Stokes solver is used for each flow calculation as in [12]. In stead, we chose XFOIL[9] for the flow calculations. XFOIL is an inviscid linear-vorticity panel method with source distributions superimposed on the airfoil and its wake allowing modeling of viscous layer influence on the potential flow. A two-equation integral boundary layer method is used to represent the viscous layer [8]. XFOIL is developed for transonic and low Reynolds number flows and is well suited for optimization because of the relative fast and robust viscous/inviscid interaction scheme.

For given angle of attack, Reynolds number and Mach number, XFOIL provides pressure distribution, lift and drag coefficients. In addition, numerous boundary layer parameters are calculated, e.g., displacement and momentum thickness, shape factor, skin friction, transition point location, etc. In XFOIL, transition is modeled by the e^n method with n = 9 as default value.

3.6 Structural analysis

Simple structural calculations were carried out on the airfoil cross section such as the airfoil thickness and mean line distributions, the airfoil maximum relative thickness, area, and area moments of inertia.

4 Design strategy

Before turning to the specific design of the airfoil family, we describe in general terms the design strategy followed. The design task or rather the optimization problem is defined by the design variables, the operating conditions, the design objectives and the constraints.

Design variables

The design variables are chosen among the control points of the B-spline describing the airfoil shape. The control points at the trailing edge are typically fixed in both the x and y directions to provide the desired trailing edge thickness. For most of the control points only the y-coordinate is a design variable to limit the number of design variables and to ensure a uniform spacing between the control points.

Operational conditions

The overall operational conditions are defined by the Reynolds number based on chord and the Mach number. The Reynolds number for an airfoil section on a wind turbine blade depends on the span-wise location and on the size of the wind turbine. Since the maximum Mach number is usually around 0.2, the flow can be considered incompressible with good approximation.

Design objectives

To allow both aerodynamic and structural objectives and off-design objectives, the objective function is defined as a linear combination of objectives, $F = \sum_{i=1}^{n} a_i f_i$, where a_i are weight factors and f_i are the different objectives.

The objectives can be both aerodynamic (e.g., lift-drag ratio for one or more angles of attack) and structural (e.g., moment of inertia of thickness at a certain chord-wise position).

The weighting of the different objectives is the responsibility of the designer and this has obviously great influence on the final design.

The objective at the design angle of attack is usually given a high weight factor to secure good performance at the design point.

Design constraints

To conclude the definition of the optimization problem, constraints are imposed on the design. To obtain the desired maximum lift coefficient and lift curve, upper and lower limits are imposed on the lift coefficient at the design angle of attack and other angles of attack, e.g., the $C_{L\max}$-angle of attack and in the post-stall region, Figure 3.

The design angle of attack, α_d should be chosen 1-2 degrees below $C_{L\max}$ to ensure a linear $C_L(\alpha)$ and low drag at angles until $C_{L\max}$. In principle, α_d can be anywhere on the linear part of the lift curve, α_d can even be a design variable.

Depending on the desired post stall characteristics, constraints can also be added to the suction side separation point, S_{sep}, that should be at the trailing edge at α_d and then move towards the leading edge just before $C_{L\max}$. To ensure a well defined stall, there should be a sudden movement in S_{sep} at $C_{L\max}$. A smooth trailing edge stall can be specified with a low negative slope for $S_{\text{sep}}(\alpha)$ in stall, whereas an abrupt stall can be achieved with a significant drop in S_{sep} towards the leading edge at stall.
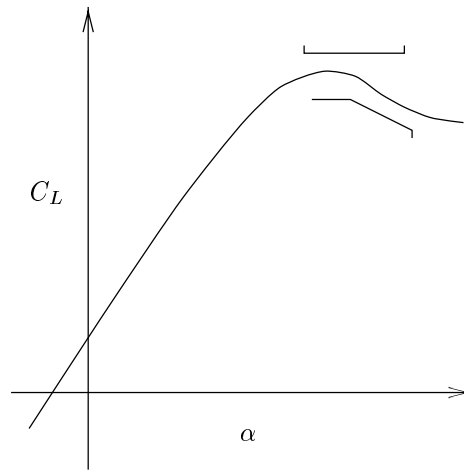
Figure 3. Constraints on the lift curve

Insensitivity to leading edge roughness is obtained by controlling the location of the transition point on the suction side, $S_{\mathrm{tr}}(\alpha)$ before and after $C_{L\mathrm{max}}$. To increase the lift-drag ratios at the angles of attack corresponding to the design objectives, S_{tr} should in general be as far downstream as possible at α_d and other angles of attack below stall. At $C_{L\mathrm{max}}$, S_{tr} should be close to the leading edge. The flow on most of the suction side would then be turbulent because of early transition and the transition points would be equally located for both smooth and rough leading edges securing minimal difference in $C_{L\mathrm{max}}$ and lift curve slopes. The transition point should remain close to the leading edge throughout the post stall region. The remaining effect from leading edge roughness would be an increase in drag.

As a structural constraint, the airfoil thickness as a function of chord-wise position is constrained to give the desired relative thickness, but also to avoid negative thickness.

Other constraints can be added to the airfoil shape or the velocity distribution, the maximum suction side velocities, structural requirements or aerodynamic requirements at other angles of attack. For development of airfoil families, constraints can ensure compatibility of both the aerodynamic characteristics and of the airfoil shapes.

To run an optimization, an initial airfoil shape is generated. This can in principle be an arbitrary shape that might be very different from the optimum shape. However, computational costs are reduced when the initial design is close to the optimum design. Side constraints are added to the design variables to ensure that they move within reasonable limits. During the optimization, the flow solver calculates the flow for all angles of attack where objectives and constraints are defined. Typically the flow is solved at a few angles of attack before stall and at several angles of attack in stall. For a reliable optimization process, convergence problems in the flow predictions should be avoided.

5 Airfoil family

In this section, we present the basis for and result of the design of the airfoil family.

5.1 Validity of geometry description

Before presenting the results of the airfoil design, we check that the geometry description is acceptable, in the sense that it should be able to represent many different airfoils with a limited number of design variables. This is done by letting the design tool minimize the geometric difference between a new design and typical wind turbine airfoils, i.e., NACA 63-418, FFA-W3-241, and DU 91-W2-250. That is, the root mean square sum of differences in y-coordinates is minimized. The results are given in Figure 4, and they show that the geometry description can reproduce the various shapes reasonably well.

(a) NACA 63-418

(b) FFA-W3-241

(c) DU 91-W2-250
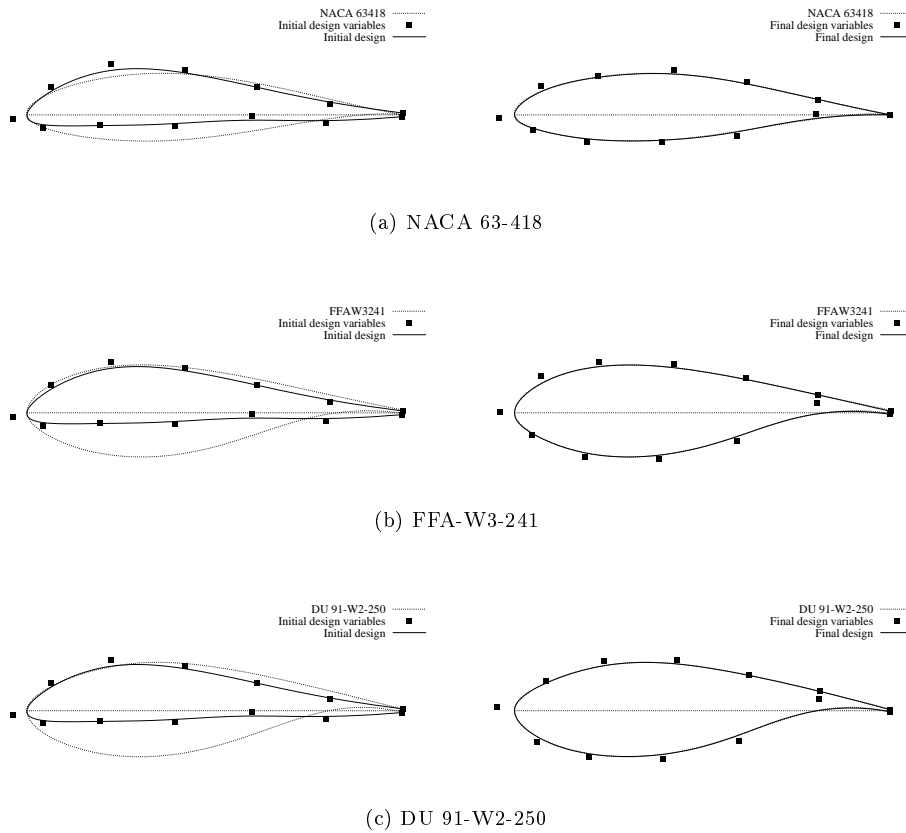
Figure 4. Geometric representation of wind turbine airfoils

On the basis of this exercise, we assume that the geometry description based on a B-spline is capable of generating a large part of the infinite numbers of possible airfoil shapes.

5.2 Design criteria

In the following, the design of 7 airfoils is described. The relative airfoil thicknesses range from 12% to 30%. The design angle of attack is 10°. The objective function is the sum of lift-drag ratios at angle of attacks of 2°, 4°, 6°, 8°, and 10°. The weight factors are all the same, but in a sense the lift-drag ratio at 10° has the largest weight factor since it is the largest and the optimization algorithm would tend to optimize here. Furthermore, a high lift-drag ratio at 10° leads to high lift-drag ratios also at lower angles of attack. The constraints for the three thin airfoils are given in Table 1 and in Table 2 for the four thick airfoils.

For all seven airfoils, the upper and lower limits on the lift curve are identical. The design lift at 10° is between 1.53 and 1.55 and the $C_{L\max}$ of 1.65 should be reached at about 11°.

The separation point, S_{sep} on the suction side is fixed to the trailing edge until $C_{L\max}$ is reached. Separation for a turbulent boundary layer was estimated from $H < 2.8$ as separation criterion as in [27], where H is the boundary layer shape factor.

The constraints on the suction side transition point differ for the thin and thick airfoils. For RISØ–A–12, RISØ–A–15, and RISØ–A–18, the transition point, S_{tr} is located on the first 7% of the chord for angles of attack above the $C_{L\max}$-angle. For the remaining thicker airfoils, the transition point is on the first 10% of the chord.

For RISØ–A–24, RISØ–A–27, and RISØ–A–30, an additional constraint is that the flow on the suction side decelerates from $0.4 \leq x/c \leq 0.9$ for $\alpha = 0°$.

Table 1. Constraints for RISØ–A–12, RISØ–A–15 and RISØ–A–18.

α	10.0°	10.5°	11.0°	11.5°	12.0°	12.5°	13.0°	13.5°
$C_{L\min}$	1.53		1.64	1.64	1.62	1.60	1.58	1.56
$C_{L\max}$	1.55		1.65	1.65	1.65	1.65	1.65	1.65
$S_{\mathrm{sep,min}}$	0.999	0.999	0.999					
$S_{\mathrm{tr,max}}$				0.07	0.07	0.07	0.07	0.07

Table 2. Constraints for RISØ–A–21, RISØ–A–24†, RISØ–A–27† and RISØ–A–30†.

α	10.0°	10.5°	11.0°	11.5°	12.0°	12.5°	13.0°	13.5°
$C_{L\min}$	1.53		1.64	1.64	1.62	1.60	1.58	1.56
$C_{L\max}$	1.55		1.65	1.65	1.65	1.65	1.65	1.65
$S_{\mathrm{sep,min}}$	0.999	0.999	0.999					
$S_{\mathrm{tr,max}}$				0.10	0.10	0.10	0.10	0.10

†$dvi_s \leq 0$ for $\alpha = 0°$ and $0.4 \leq x/c \leq 0.9$

In Table 3, the operational conditions are given together with selected properties of the resulting airfoil design. The operational conditions are the Reynolds numbers and the Mach numbers corresponding to a typical 600kW wind turbine. The Reynolds and Mach numbers are relatively high for the thinner airfoils in the tip region and on the mid section but lower for the thicker airfoil used in the root region.

The maximum lift coefficients (according to XFOIL) are also given for both clean and dirty conditions (i.e., rough leading edge). In calculations with rough leading

edge, the transition points for the suction and pressure sides were fixed to 1% and 10%, respectively as in [4]. We see that going from clean to dirty conditions $C_{L\max}$ drops about 10% for RISØ–A–12 to RISØ–A–24 and about 15% for RISØ–A–27 and RISØ–A–30.

Table 3. Operational conditions and selected properties the airfoil design

	t/c	$\text{Re} \times 10^{-6}$	Ma	$C_{L\max}(\alpha)$†	$C_{L\max}(\alpha)$‡
RISØ–A–12	12%	3.00	0.20	1.65(11.5°)	1.51(10.0°)
RISØ–A–15	15%	3.00	0.16	1.64(11.5°)	1.52(11.0°)
RISØ–A–18	18%	3.00	0.11	1.64(12.0°)	1.53(11.5°)
RISØ–A–21	21%	3.00	0.09	1.65(12.0°)	1.50(11.0°)
RISØ–A–24	24%	2.75	0.07	1.65(12.0°)	1.48(10.5°)
RISØ–A–27	27%	2.75	0.07	1.65(12.0°)	1.39(11.0°)
RISØ–A–30	30%	2.50	0.05	1.65(12.0°)	1.37(11.0°)

†free transition, ‡fixed transition

5.3   Geometric properties

The airfoil shapes are given in Figures 5 and 6. Geometrically, RISØ–A–18 to RISØ–A–30 are clearly a family, whereas RISØ–A–12 and RISØ–A–15 do not look like their thicker relatives. The entire family is characterized by a sharp nose.

For RISØ–A–27 and RISØ–A–30 the rear part of the suction side is slightly wavy, which it might be possible to remove if not for anything else as for aesthetic reasons with out compromising aerodynamic performance. This has not been tried in this work but it is an obvious possibility for future improvement of the design.

RISØ-A-XX

Figure 5. Airfoil shapes

RISØ-A-12

RISØ-A-15

RISØ-A-18

RISØ-A-21

RISØ-A-24

RISØ-A-27

RISØ-A-30
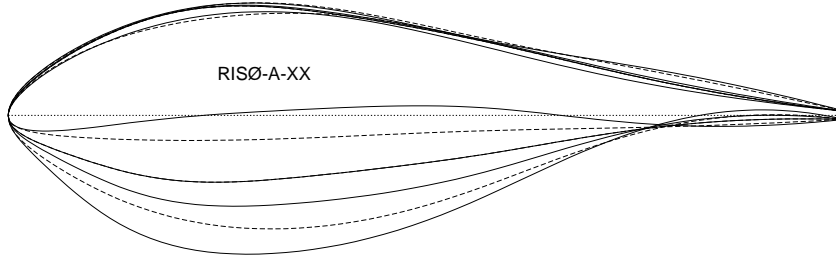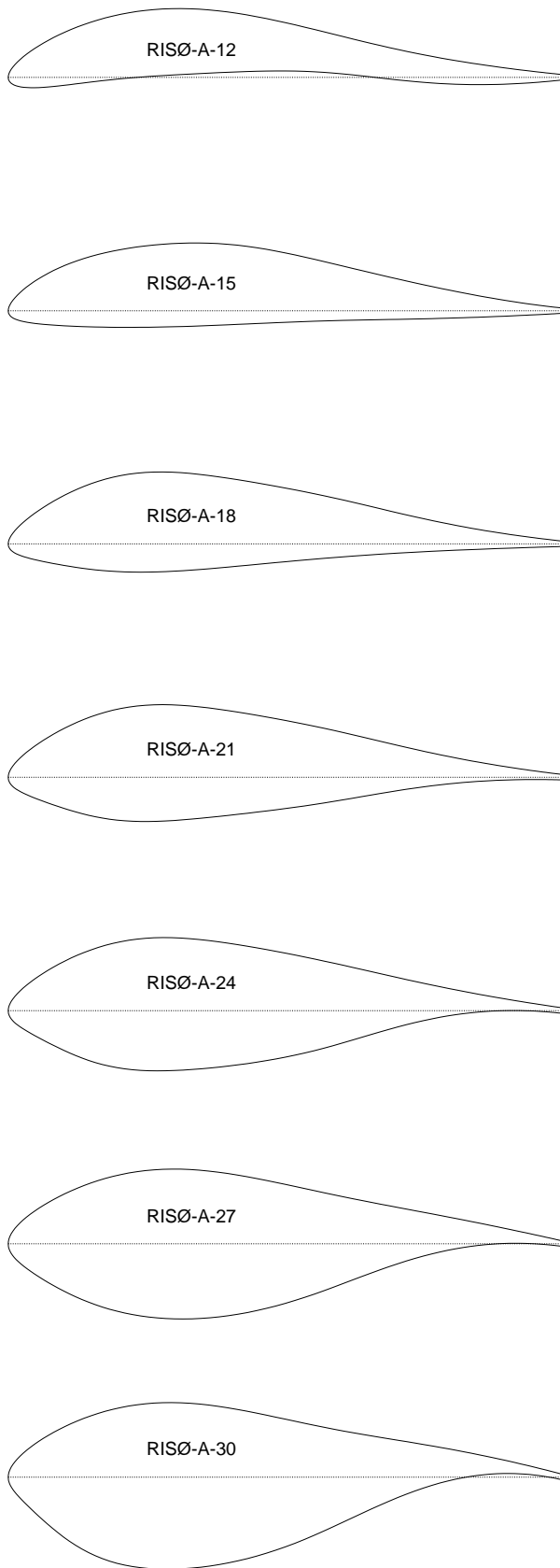
Figure 6. Airfoil shapes, revisited

5.4 Aerodynamic properties

The airfoil polars (C_L,C_D, and the suction side transition point, S_{tr})are given in Figures 7 to 9 for both clean and dirty conditions. Aerodynamically, they all look a like. This is obviously due to the fact that the aerodynamic constraints are identical more-or-less. But, again, the two thinner airfoils are slightly different from the rest, judging from the appearance of the lift and drag curves. RISØ–A–27 and RISØ–A–30 are also special with their 15% drop in $C_{L\text{max}}$ going from clean to dirty conditions. All the airfoils have a distinct and well-defined stall with a linearly increasing C_L until the design angle of attack.

The pressure distributions for $\alpha = 8.5°$, Figure 10 underline the *subrelations* within the family. The family consists of thin members (RISØ–A–12 and RISØ–A–15), intermediate members (RISØ–A–18 to RISØ–A–24), and thick members (RISØ–A–27 and RISØ–A–30). The pressure distributions are all characterized by a narrow suction peak that appears around 8° when the stagnation point moves slightly downstream on the leading edge part of the pressure side.. This causes the flow to accelerate around the sharp nosed leading edge of the airfoils. The suction peak is not present at low angles of attack but at higher angles of attack it eventually provokes transition from laminar to turbulent flow on the front part of the airfoils. In Figure 10, the transition points on the suction side are all around $x/c = 0.3$.
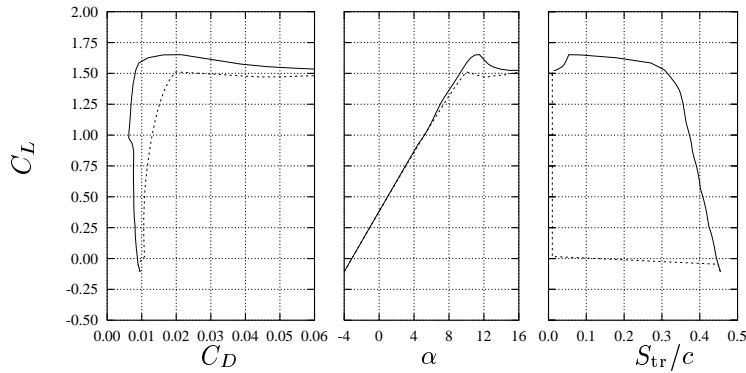
(a) RISØ–A–12
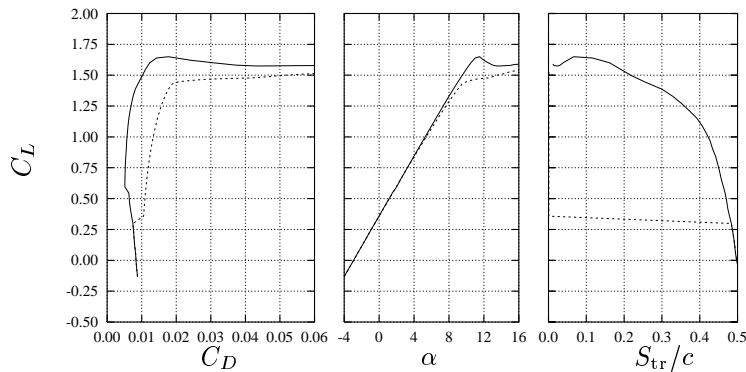
(b) RISØ–A–15

Figure 7. XFOIL polars. Solid line: free transition, dashed line: fixed transition.
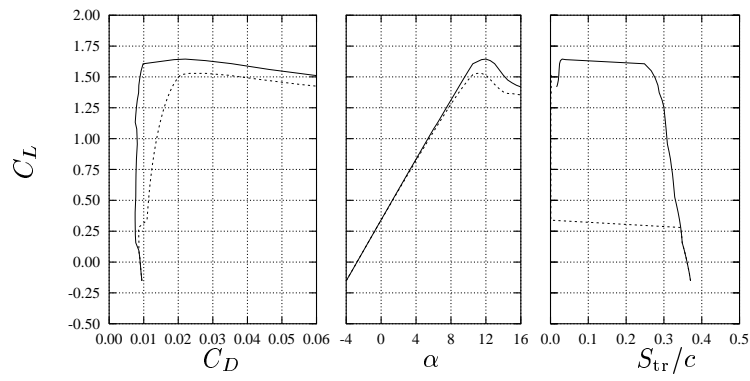
(a) RISØ–A–18
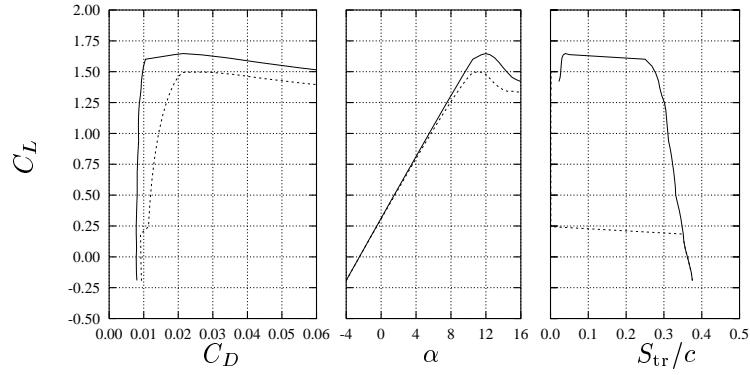
(b) RISØ–A–21
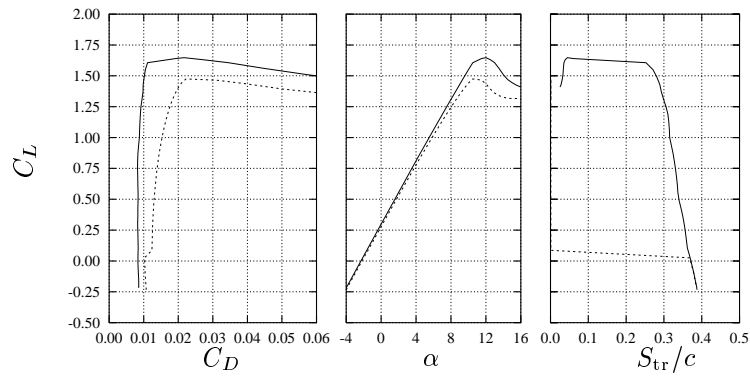
(c) RISØ–A–24

*Figure 8. **XFOIL** polars. Solid line: free transition, dashed line: fixed transition.*
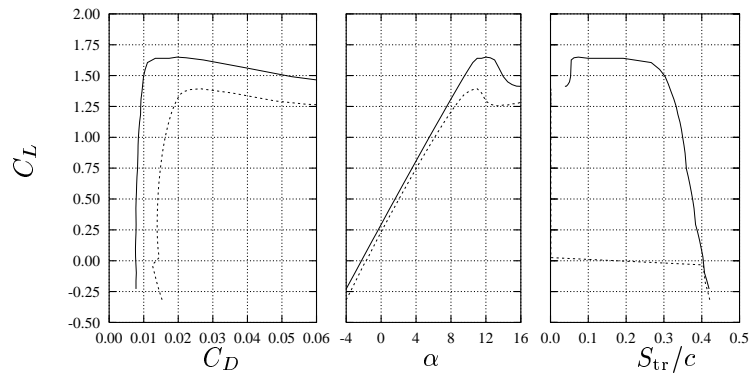
(a) RISØ–A–27
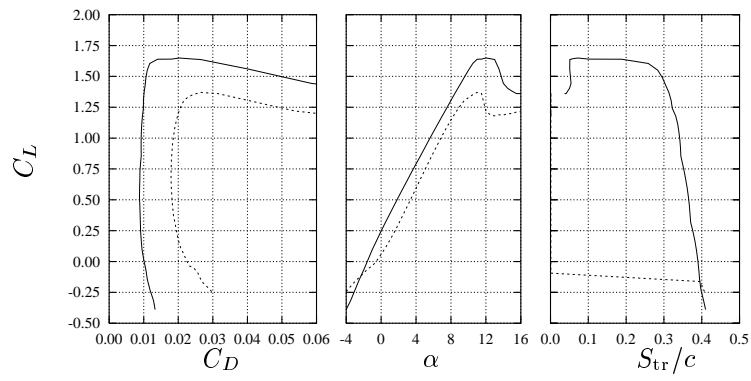
(b) RISØ–A–30

Figure 9. XFOIL polars. Solid line: free transition, dashed line: fixed transition.
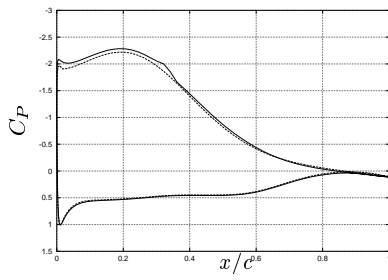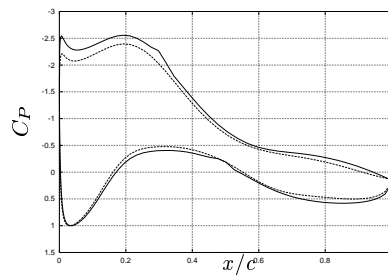
(a) RISØ–A–12
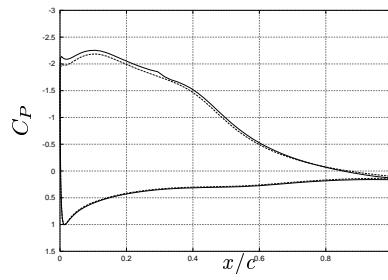
(b) RISØ–A–15
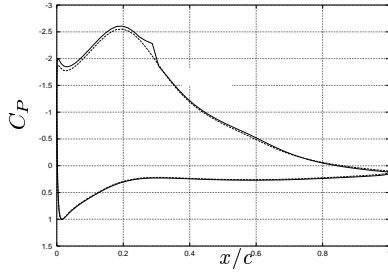
(c) RISØ–A–18
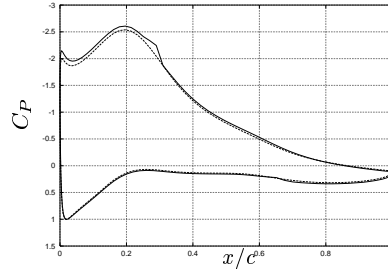
(d) RISØ–A–21
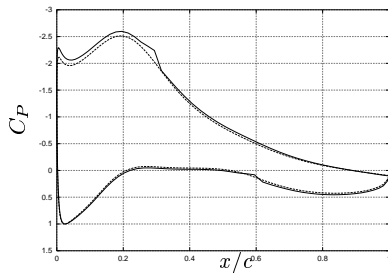
(e) RISØ–A–24
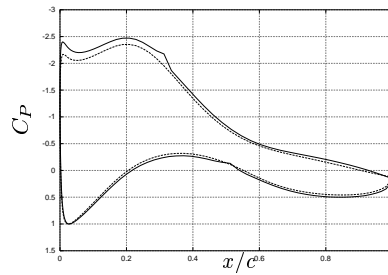
(f) RISØ–A–27

(g) RISØ–A–30

Figure 10. **XFOIL** *pressure distributions for* $\alpha = 8.5°$*. Solid line: free transition, dashed line: fixed transition.*

5.5 Comparison of XFOIL and EllipSys2D predictions

In the design process we have used XFOIL, which often overestimates $C_{L\max}$ and give poor results in the post stall region [21]. Therefore, as an extra check, the airfoil designs are evaluated with EllipSys2D, a Navier-Stokes solver [28] with the $k - \omega$ SST turbulence model [23] and the Michel transition criterion [24].

In Figures 11 to 17 the C_L and C_D predictions of XFOIL and EllipSys2D with both free transition and fixed transition are compared. That is, (a)the free transition predictions of XFOIL are compared to the free transition predictions of EllipSys2D and (b) the fixed transition predictions of XFOIL are compared to the fully turbulent predictions of EllipSys2D. By fixing the transition point at the leading edge, the depositing of dirt and bugs is simulated. This comparison goes to show if we would get a completely different design if we used another flow solver than XFOIL. Note, that the EllipSys2D predictions are for $\alpha = -4°, 0°, 4°, 8°, 9°, 10°, 11°, 12°, 13°, 14°, 15°, 16°$ whereas the less expensive XFOIL predictions are for α from $-4°$ to $16°$ for every $0.5°$.

The agreement between the XFOIL and EllipSys2D results is good for the computations with fixed transition (dirty conditions), whereas the correspondence for free transition (clean conditions) is not good for RISØ–A–24, RISØ–A–27, and RISØ–A–30. This is due to bad performance of the turbulence and the transition model in stall.

Since the designs are based on calculations with free transition, this comparison suggests that the designs would have been identical had we used EllipSys2D instead of XFOIL for RISØ–A–12, RISØ–A–15, RISØ–A–18, and perhaps RISØ–A–21. For RISØ–A–24,RISØ–A–27, and RISØ–A–30 using EllipSys2D as aerodynamic analysis tool would have given different but not necessarily better designs compared to the present ones.
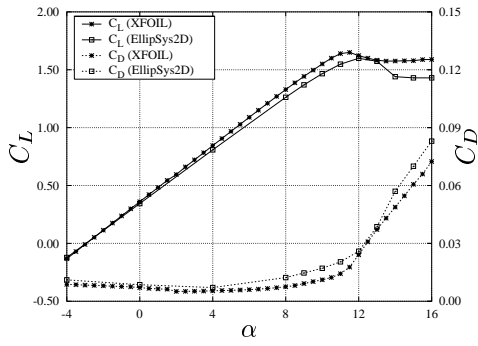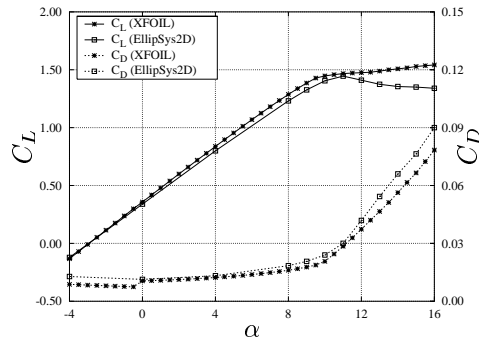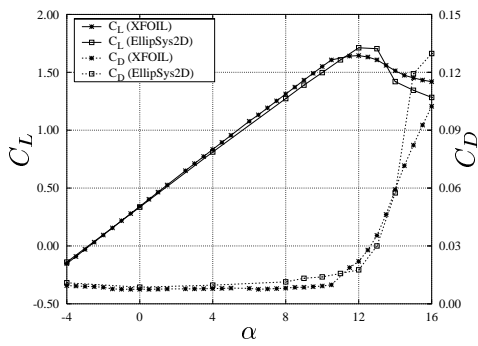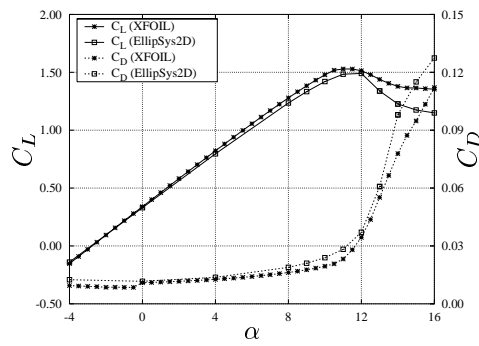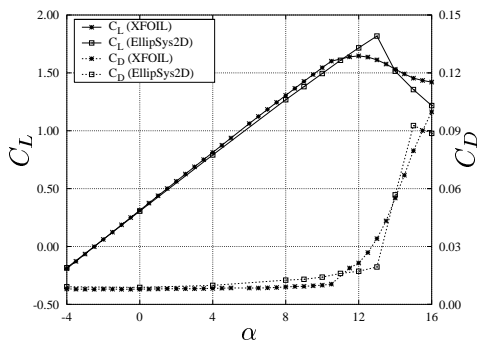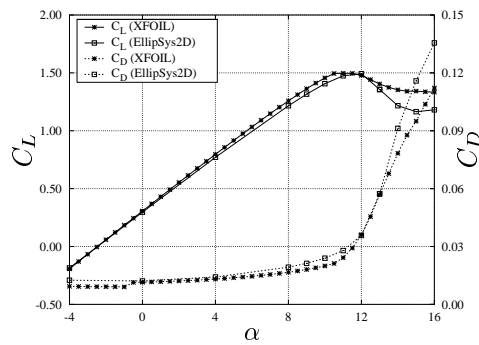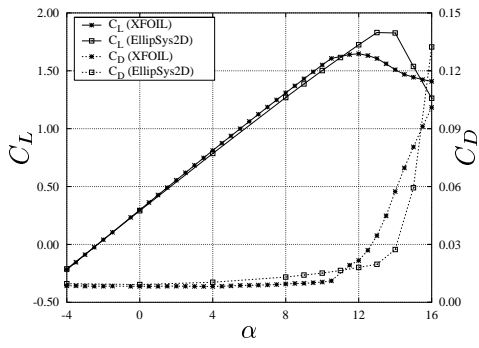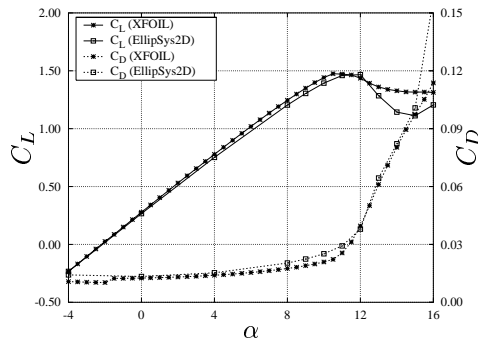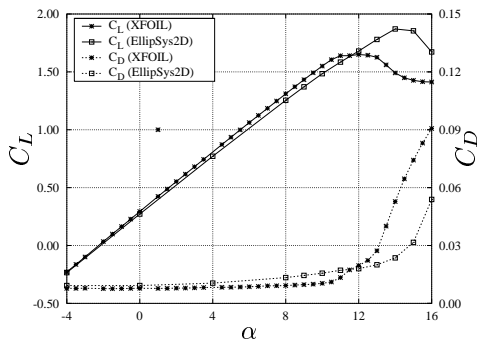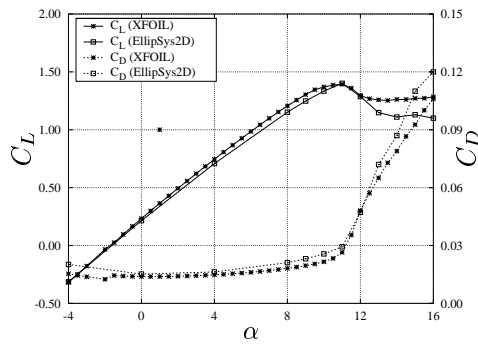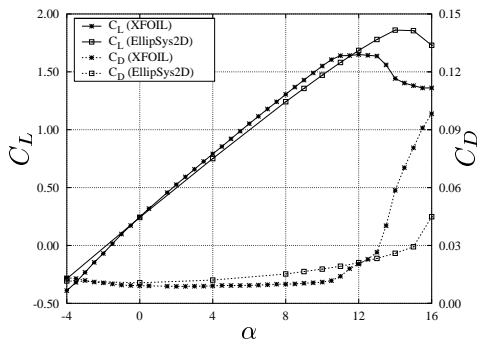

(a) Free transition   (b) Fixed transition
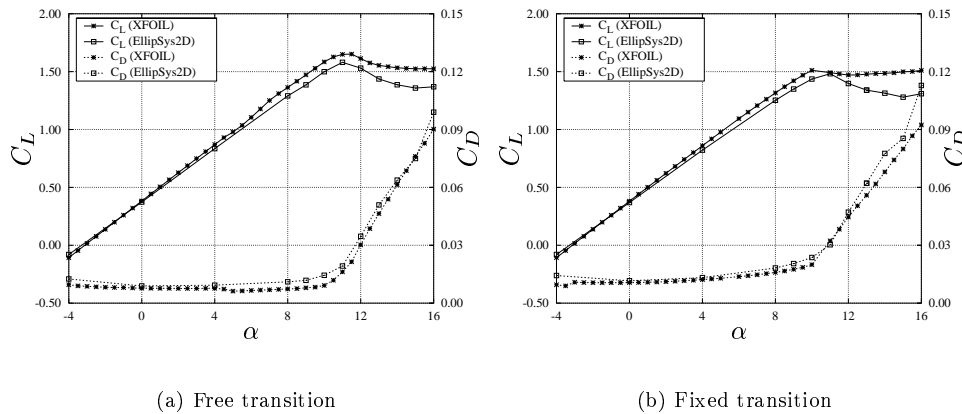
Figure 11. Comparison of XFOIL and EllipSys2D predicted C_L and C_D for RISØ–A–12

(a) Free transition   (b) Fixed transition

Figure 12. *Comparison of XFOIL and EllipSys2D predicted C_L and C_D for RISØ–A–15*

(a) Free transition   (b) Fixed transition

Figure 13. *Comparison of XFOIL and EllipSys2D predicted C_L and C_D for RISØ–A–18*

(a) Free transition   (b) Fixed transition

Figure 14. *Comparison of XFOIL and EllipSys2D predicted C_L and C_D for RISØ–A–21*

(a) Free transition (b) Fixed transition

Figure 15. Comparison of XFOIL and EllipSys2D predicted C_L and C_D for RISØ–A–24
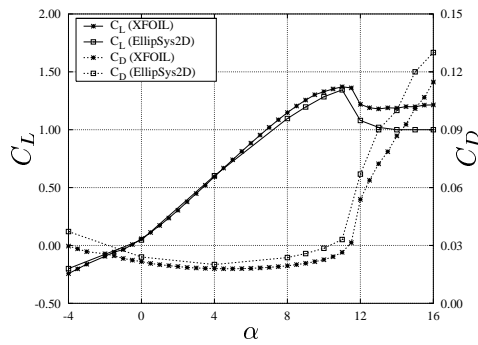

(a) Free transition (b) Fixed transition

Figure 16. Comparison of XFOIL and EllipSys2D predicted C_L and C_D for RISØ–A–27

(a) Free transition (b) Fixed transition

Figure 17. Comparison of XFOIL and EllipSys2D predicted C_L and C_D for RISØ–A–30

5.6 Comparison of clean and dirty performance

In Figures 18–24 the C_L and C_D predictions with free and fixed transition for both XFOIL and EllipSys2D are compared. That is, (a)XFOIL predictions based on free transition are compared with XFOIL predictions based on fixed transition and (b)EllipSys2D predictions based on free transition are compared with EllipSys2D predictions based on fixed transition. This comparison illustrates the decrease in $C_{L\max}$ and the increase in C_D going from clean to dirty conditions.

Qualitatively, XFOIL and EllipSys2D give the same picture of going from clean to dirty conditions for RISØ–A–12 to RISØ–A–21, whereas the inadequacy of the turbulence and transition modelling in the separated region give different pictures for RISØ–A–24, RISØ–A–27, and RISØ–A–30.
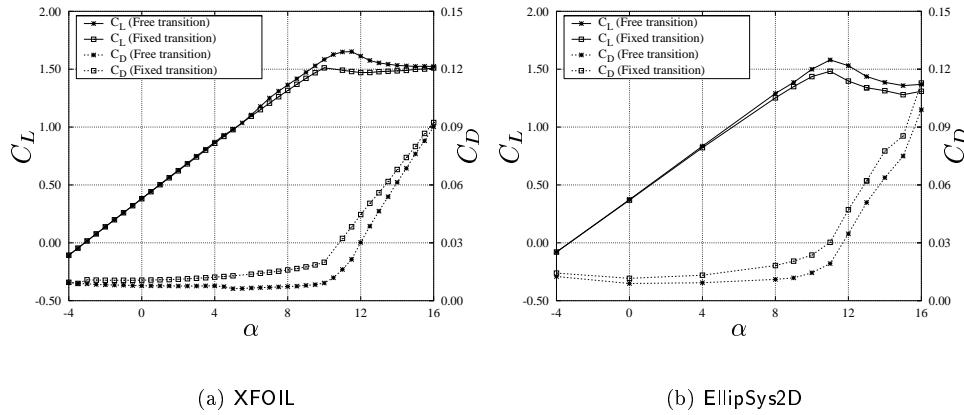

(a) XFOIL   (b) EllipSys2D

Figure 18. Comparison of C_L and C_D predictions with free and fixed transition for RISØ–A–12
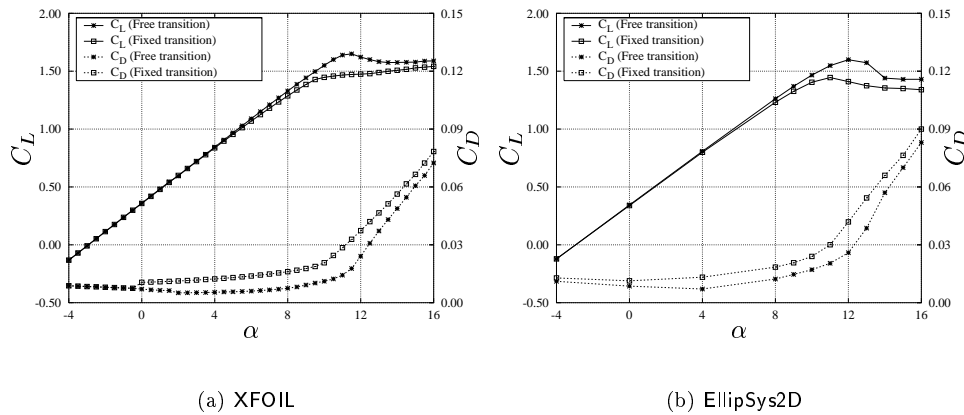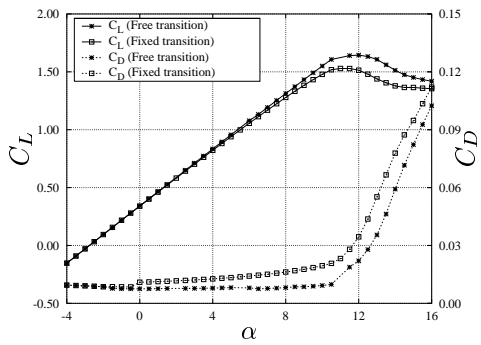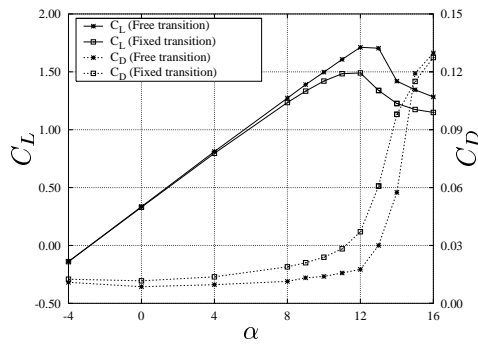

(a) XFOIL   (b) EllipSys2D

Figure 19. Comparison of C_L and C_D predictions with free and fixed transition for RISØ–A–15
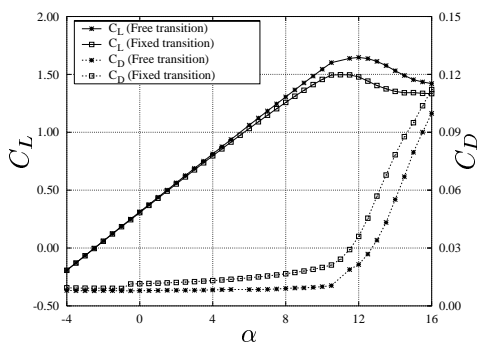
(a) XFOIL   (b) EllipSys2D

Figure 20. Comparison of C_L and C_D predictions with free and fixed transition for RISØ–A–18

(a) XFOIL   (b) EllipSys2D

Figure 21. Comparison of C_L and C_D predictions with free and fixed transition for RISØ–A–21

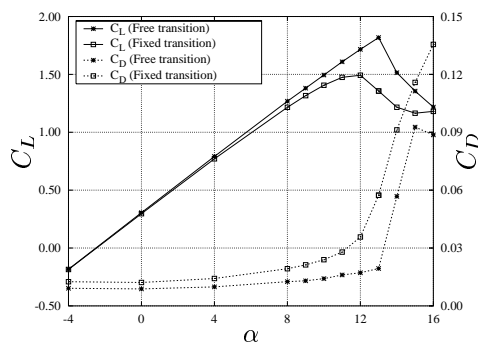(a) XFOIL   (b) EllipSys2D

Figure 22. Comparison of C_L and C_D predictions with free and fixed transition for RISØ–A–24
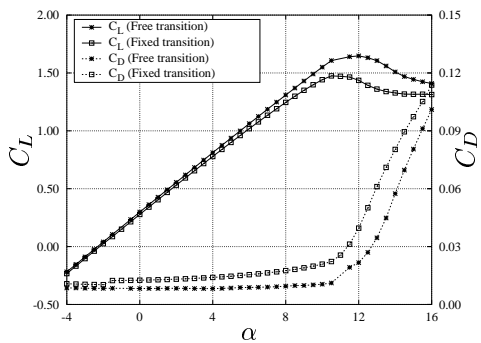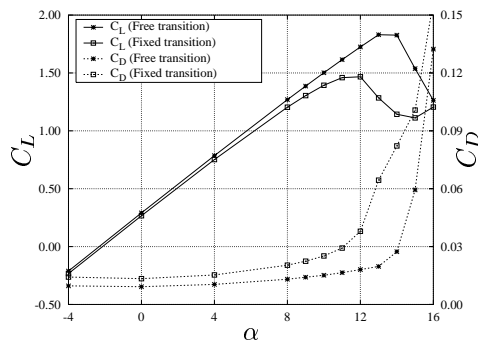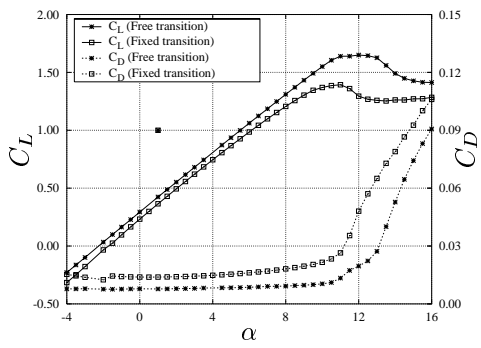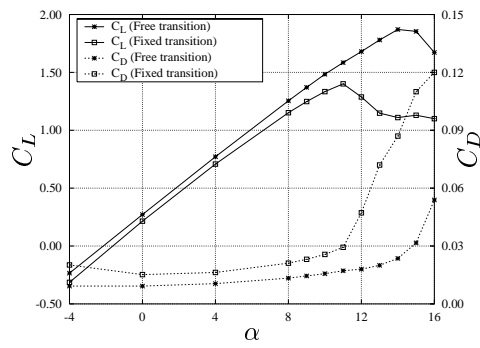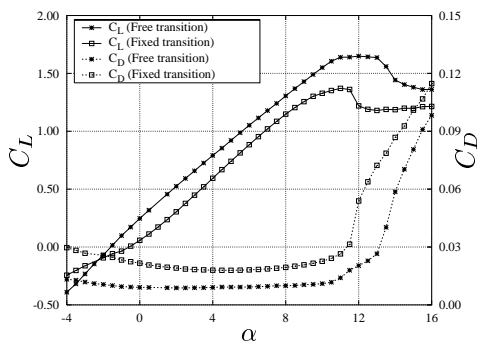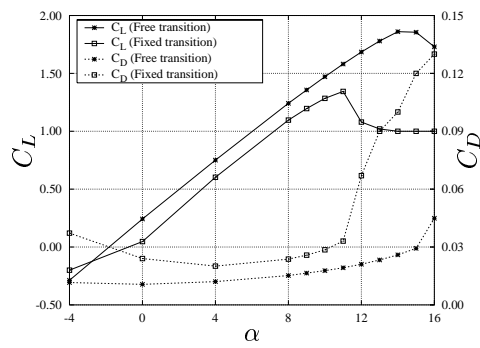
(a) XFOIL (b) EllipSys2D

Figure 23. Comparison of C_L and C_D predictions with free and fixed transition for RISØ–A–27

(a) XFOIL (b) EllipSys2D

Figure 24. Comparison of C_L and C_D predictions with free and fixed transition for RISØ–A–30

6 Conclusion

A method for design of wind turbine airfoils was developed. The design method is based on direct numerical optimization of airfoil shapes described by B-splines subject to aerodynamic and structural objectives and constraints.

The capabilities of the method was demonstrated by the design of a complete airfoil family composed of 7 airfoils ranging from 12% to 30% in relative thickness. The airfoils were designed for Reynolds and Mach numbers representative of a 600 kW wind turbine. Aerodynamically, the airfoils perform identically, i.e., they have high lift-drag ratio until $C_{L\mathrm{max}}$ is reached, a design angle of attack of 10°, a design lift between 1.53 and 1.55 and maximum lift around 1.65 at 11°according to XFOIL. Beyond α=11°, the lift is constrained to lie within a band to secure a smooth post stall behavior. Moreover, for angles of attack above the maximum lift angle the transition point is located on the first 10% of the airfoil. This constraint is put on the design to obtain insensitivity to leading edge roughness for $C_{L\mathrm{max}}$. Computations with forced transition on the leading edge show as a measure of the insensitivity to leading edge roughness that the maximum lift coefficient does not drop more than 10% to 15% depending on the relative thickness. A geometrical feature of the airfoil family is the sharp nose region that rapidly accelerates the flow and generates a suction peak that eventually leads to transition close to the leading edge.

The airfoil designs have been checked with the CFD code EllipSys2D and the results are in good agreement with the results of XFOIL except for the free transition computations for the thicker airfoils RISØ–A–24,RISØ–A–27, and RISØ–A–30. The discrepancies are due to the poor performance of the turbulence and transition models in post stall. But the comparison between XFOIL and EllipSys2D suggests that the design for RISØ–A–12 to RISØ–A–21 had been the same with the use of EllipSys2D instead of XFOIL.

The present design method and the airfoil family itself provides an good basis for further improvements in the design. For some of the airfoils it should be examined if the wavy rear part of the suction side can be straightened out with out compromising the aerodynamic performance. Additionally, the geometric compatibility between the different airfoils might also be improved.

References

[1] ABBOTT, I. H., AND VON DOENHOFF, A. E. *Theory of Wing Sections*. Dover Publications, Inc., 1959.

[2] ALY, S., OGOT, M., AND PELZ, R. Stochastic Approach to Optimal Aerodynamic Shape Design . *Journal of Aircraft 33*, 5 (Sep-Oct 1996), 956–961.

[3] BAK, C., MADSEN, H. A., FUGLSANG, P., AND RASMUSSEN, F. Double Stall. Risø-R-1043(EN), Risø National Laboratory, Denmark, 1998.

[4] BJÖRK, A. Airfoil design for variable RPM horizontal axis wind turbines. In *EWEC'89* (Glasgow, Scotland, 1989).

[5] CHATTOPADHYAY, A., PAGALDIPTI, N., AND CHANG, K. T. A Design Optimization Procedure for Efficient Turbine Airfoil Design. *J. Computers Math. Applic. 26*, 4 (1993), 21–31.

[6] CHAVIAROPOULOS, P., BOURAS, B., LEOUTSAKOS, G., AND PAPAILIOU, K. D. Design of Optimized Profiles for Stall Regulated HAWTs Part 1: Design Concepts and Method Formulation. *Wind Engineering 17*, 6 (1993), 275–287.

[7] DE BOOR, C. *A Practical Guide to Splines*. Springer-Verlag, New York, 1978.

[8] DRELA, M. XFOIL: An Analysis and Design system for Low Reynolds Number Airfoils. In *Low Reynolds Number Aerodynamics* (1989), vol. 54 of *Springer-Verlag Lec. Notes in Eng.*

[9] DRELA, M., AND GILES, M. B. Viscous-inviscid analysis of transonic and low Reynolds number airfoils. *AIAA Journal 25*, 10 (1987).

[10] DULIKRAVICH, G. S. Aerodynamic Shape Design and Optimization: Status and Trends. *J. of Aircraft 29*, 6 (Nov-Dec 1992), 1020–1026.

[11] EPPLER, R., AND SOMERS, D. M. A Computer Program for the Design and Analysis of Low-Speed Airfoils. Tech. rep., NASA TM 80210, 1980.

[12] EYI, S., LEE, K. D., ROGERS, S. E., AND KWAK, D. High-Lift Design Optimization Using Navier-Stokes Equations. *Journal of Aircraft 33*, 3 (May-June 1996), 499–504.

[13] FUGLSANG, P., AND MADSEN, H. A. Numerical optimization of wind turbine rotors. In *EUWEC'96* (Göteborg, Sweden, 1996).

[14] HAGER, J. O., EYI, S., AND LEE, K. D. Two-point transonic airfoil design using optimization for improved off-design performance. *Journal of Aircraft 31*, 5 (1994).

[15] HENNE, P. A. E. *Applied Computational Aerodynamics*. American Institute of Aeronautics and Astronautics, Inc., 1989.

[16] HICKS, R. M., MURMAN, E., AND VANDERPLAATS, G. N. An Assessment of Airfoil Design by Numerical Optimization. *NASA TM X-3092* (July 1974), 31 p.

[17] HILL, D. M., AND GARRAD, A. D. Design of Aerofoils for Wind Turbine Use. In *IEA Symposium on Aerodynamics of Wind Turbines* (Lyngby, Denmark, 1988).

[18] JAMESON, A. Aerodynamic Design Via Control Theory. Tech. Rep. Rept. 88-64, Inst. for Computer Applications in Science and Engineering, NASA Langley, Hampton, VA., 1988.

[19] LIEBECK, R. H. Design of Subsonic Airfoils for High Lift. In *AIAA 9th Fluid and Plasma Dynamics Conference* (San Diego, Californien, July 1976).

[20] LIGHTHILL, M. J. A New Method of Two-Dimensional Aerodynamic Design . Tech. Rep. R & M Report 2112, Aeronautical Research Council, London, June 1945.

[21] MADSEN, H. A., AND FILIPPONE, A. Implementation and Test of the XFOIL Code for Airfoil Analysis and Design. Risø-R-644(EN), Risø National Laboratory, Denmark, 1995.

[22] MANGLER, K. W. Design of Airfoil Sections. Jahrbuch Goettingen FRG, Deutscher Luftfahrforschung, 1938.

[23] MENTER, F. R. Zonal Two Equation $k - \omega$ Turbulence Models for Aerodynamic Flows. *AIAA Paper 93-2906* (1993).

[24] MICHEL, R. Etude de la transition sur les profiles d'aile. Tech. Rep. Report 1/1578-A, ONERA, 1952. See White F.M., Viscous fluid flow, p. 442.

[25] OBAYASHI, S., AND TAKANASHI, S. Genetic Optimization of Target Pressure Distributions for Inverse Design methods. *AIAA Journal 34*, 5 (May 1996).

[26] PRESS, W. H., FLANNERY, B. P., TEUKOLSKY, S. A., AND VETTERLING, W. T. *Numerical Recipes: The Art of Scientific Computing.* Cambridge University Press, 1986.

[27] SELIG, M. S., AND MAUGHMER, M. D. Multipoint Inverse Airfoil Design Method Based on conformal Mapping. *AIAA Journal 30*, 5 (1992).

[28] SØRENSEN, N. N. General Purpose Flow Solver Applied to flow over Hill. Risø-R-827(EN), Risø National Laboratory, Denmark, 1995.

[29] TANGLER, J. L.; SOMERS, D. M. Status of the Special-Purpose Airfoil Families. In *WINDPOWER '87, San Fransisco* (1987).

[30] TIMMER, W., AND VAN ROOY, R. Thick airfoils for HAWTs. *Journal of Wind Engineering and Industrial Aerodynamics 39* (1992).

[31] VANDERPLAATS, G. N. *Numerical Optimization Techniques for Engineering Design: With applications.* McGraw-Hill Book Company, 1984.

Title and author(s)

Design of the Wind Turbine Airfoil Family RISØ–A–XX

Kristian S. Dahl, Peter Fuglsang

Abstract (Max. 2000 char.)

A method for design of wind turbine airfoils is presented. The design method is based on direct numerical optimization of a B-spline representation of the airfoil shape. For flexibility, the optimization algorithm relies on separate, stand alone tools for the analysis of aerodynamic and structural properties. The panel method based XFOIL is used during the optimization whereas the Navier-Stokes solver EllipSys2D is used in the evaluation of the results.

The method is demonstrated by the design of an airfoil family composed of 7 airfoils ranging in thickness from 12% to 30%. The design is based on Reynolds and Mach numbers representative of a 600 kW wind turbine. The airfoils are designed to have maximum lift-drag ratio until just below stall, a design lift coefficient of about 1.55 at an angle of attack of 10° and a maximum lift coefficient of 1.65. The airfoils are made insensitive to leading edge roughness by securing that transition from laminar to turbulent flow on the suction side occurs close to the leading edge for post stall angles of attack.

The design method and the airfoil family provides a sound basis for further enhancing the characteristics of airfoils for wind turbines and to tailor airfoils for specific rotor sizes and power regulation principles.

Descriptors INIS/EDB

AERODYNAMICS; AIRFOILS; DESIGN; OPTIMIZATION; TURBINE BLADES; HORIZONTAL AXIS TURBINES; TWO-DIMENSIONAL CALCULATIONS